THE ASTRONOMICAL JOURNAL, 117:671–676, 1999 February

HUBBLE SPACE TELESCOPE IMAGING POLARIMETRY OF THE GRAVITATIONAL LENS FSC 10214+4724[1]

HIEN T. NGUYEN,[2] PETER R. EISENHARDT,[2] MICHAEL W. WERNER,[2] ROBERT GOODRICH,[3] DAVID W. HOGG,[4,5] LEE ARMUS,[6] B. T. SOIFER,[7] AND G. NEUGEBAUER[7]

Received 1998 August 31; accepted 1998 October 14

ABSTRACT

We present imaging polarimetry of the extremely luminous, redshift 2.3 *IRAS* source FSC 10214+4724. The observations were obtained with *HST*'s Faint Object Camera in the F437M filter, which is free of strong emission lines. The 0.″7 long arc is unresolved to 0.″04 FWHM in the transverse direction and has an integrated polarization of 28% ± 3%, in good agreement with ground-based observations. The polarization position angle varies along the arc by up to 35°. The overall position angle is 62° ± 3° east of north. No counterimage is detected to $B = 27.5$ mag (3 σ), giving an observed arc to counterimage flux ratio greater than 250, considerably greater than the flux ratio of 100 measured previously in the I band. This implies that the configuration of the object in the source plane at the B band is different from that at I band and/or that the lensing galaxy is dusty.

Key words: galaxies: elliptical and lenticular, cD — gravitational lensing — infrared radiation — quasars: general — quasars: individual (FSC 10214+4724)

1. INTRODUCTION

With a redshift of $z = 2.286$, FSC 10214+4724 remains the most distant object identified in the *IRAS* database. At the time of its initial discovery in 1991 (Rowan-Robinson et al. 1991), it was estimated to have a luminosity well in excess of $\sim 10^{14}\ L_\odot$, most of which emerged in the far-infrared. Subsequent *HST* observations of FSC 10214+4724 (Eisenhardt et al. 1996, hereafter E96) with F814W (roughly I band, center wavelength of 814 nm) have shown conclusively that the source is gravitationally lensed by a foreground elliptical galaxy, reducing its intrinsic luminosity to $\sim 2 \times 10^{13}\ L_\odot$. The redshift of the lensing galaxy has not yet been measured with certainty, but a value of 0.9 is favored by E96 and Lacy, Rawlings, & Serjeant (1998). Millimeter and submillimeter line and continuum observations have shown that FSC 10214+4724 contains huge amounts of interstellar dust and gas and have raised the possibility that it is powered by a massive starburst (Downes, Solomon, & Radford 1995; Rowan-Robinson et al. 1993; Scoville et al. 1995). Visual spectropolarimetry (Goodrich et al. 1996, hereafter G96) has revealed both a highly polarized (25% at 0.44 μm) continuum and polarized broad wings on the otherwise unpolarized emission lines. This is the polarimetric signature of a dust-embedded quasar, hidden from direct view but seen in reflection via scattering off of favorably placed cloud(s). Therefore, both stellar and nonthermal energy sources probably contribute to the luminosity of this object (Kroker et al. 1996; Lacy et al 1998).

The present program makes use of the intervening gravitational lens as a microscope to study the structure of the inner regions of the quasar. At the F814W bandpass, the magnification appears to be quite high (~100; E96) suggesting that the background source is extremely close to a caustic of the lensing potential, so that small changes in the source position or size with wavelength will lead to differences in the position and structure of the image that could be resolved with *HST*. The principal features of the lensed image at F814W are a 0.″7 long arc, which is unresolved (<0.″06) in the transverse direction, and an unresolved counterimage, about 1.″6 away, with about 1% of the total flux of the arc. The absolute and relative positions of the arc and the counterimage, the extent and structure of the arc, and the relative brightness of the arc and the counterimage are all sensitive to the structure of the source at the observed wavelength and its position relative to the caustic of the lensing potential (E96).

This paper reports the results of imaging polarimetry of FSC 10214+4724, carried out in the continuum using filter F437M (roughly B band, center wavelength of 437 nm) with *HST*'s Faint Object Camera (FOC). Subsequent papers will report the results of *HST* imaging of the source in narrow bands centered on a number of emission lines, providing information on the spatial distribution of gas in the narrow-line region of the quasar.

At the FSC 10214+4724 redshift of $z = 2.286$, one 0.″014 FOC pixel subtends 100(60) h^{-1} pc for $q = 0(0.5)$, where $h = H_0/100$ km s^{-1} Mpc^{-1} (where not otherwise specified, we assume $H_0 = 50$ km s^{-1} Mpc^{-1} and $q = 0.5$). The FWHM of *HST*'s point spread function (PSF) at F437M is 0.″042. Hereafter, F437M and F814W are interchangeably referred to as B and I band, respectively.

2. OBSERVATIONS AND REDUCTION

Imaging polarimetry was performed through three separate polarizers, referred to as POL0, POL60, and

[1] Based on observations made with NASA/ESA *Hubble Space Telescope*, obtained at the Space Telescope Science Institute, which is operated by AURA, Inc., under NASA contract NAS 5-26555.

[2] MS 169-506, Jet Propulsion Laboratory, California Institute of Technology, Pasadena, CA 91109; hien@cougar.jpl.nasa.gov.

[3] California Association for Research in Astronomy, 65-1120 Mamalahoa Highway, Kamuela, HI 96743.

[4] Institute for Advanced Study, Olden Lane, Princeton, NJ 08540.

[5] Hubble Fellow.

[6] SIRTF Science Center, California Institute of Technology, Pasadena, CA 91125.

[7] Division of Physics, Math and Astronomy, California Institute of Technology, Pasadena, CA 91125.

POL120, where the number indicates the position angle with respect to the detector in an instrumental coordinate system. A total of 15 orbits (35,055 s) of polarimetry data were obtained using the F437M filter in the FOC, with 0.″014 pixel^{-1} and a field of view of 7.16 × 7.16 arcsec^2. The data were obtained in three visits. In the first visit, one orbit with each polarizer was obtained on 1997 May 19. Each orbit began with a 200 s exposure on the $B = 19$ mag star 13.″2 to the east (star A in E96), to allow registration of data in the three polarizers and to check the PSF; the remainder of each orbit was spent on the arc. In the second visit, six orbits were obtained on 1997 May 20–21, with each orbit evenly divided between the three polarizers. The position angle orientations on the sky for the second visit were the same as for the first. In the third visit, six orbits were obtained on 1997 June 29 using the same strategy as in the second visit, except that the telescope was rotated around its line of sight so that the polarizer position angles were rotated 30° counterclockwise on the sky from the first and second visits.

After standard processing provided by STScI, the FOC frames were corrected for spatial shifts introduced by the different polarizers. The shifts (∼few pixels) were determined by measuring the position of star A relative to each polarization image. Additional corrections were also applied for dithers (visits 2 and 3) and rotation (visit 3). The background for each individual frame was estimated and subsequently subtracted. The resulting frames were corrected for calibration and co-added for each visit. Following Thompson & Robinson (1995), we define the total intensity,

$$I = \frac{2(s_0 + s_{60} + s_{120})}{3}, \tag{1}$$

where s_i is the flux through each polarizer. The normalized Stokes parameters are then given by

$$q = \frac{Q}{I} = \frac{2s_0 - s_{60} - s_{120}}{s_0 + s_{60} + s_{120}}, \tag{2}$$

$$u = \frac{U}{I} = \frac{\sqrt{3}(s_{60} - s_{120})}{s_0 + s_{60} + s_{120}}, \tag{3}$$

and the fractional polarization by

$$p = \sqrt{u^2 + q^2}, \tag{4}$$

and the polarization position angle, which is measured counterclockwise from the scan direction (x-axis), by

$$\theta = \frac{1}{2} \arctan\left(\frac{u}{q}\right) + \theta_0, \tag{5}$$

where θ_0 is the zero-point offset of the polarizers' orientation with respect to the detector scan direction and is given to be −1.°4.

The overall polarization results were then obtained by averaging the Stokes parameters of the three visits.

3. RESULTS

The F437M image of FSC 10214+4724 is shown in Figure 1 (*top*), in gray scale, obtained from a straight co-add of frames from filters POL0 and POL120 for all three visits. These POL0 and POL120 data had a diffraction-limited PSF with a FWHM of 0.″042. The POL60 data had a degraded PSF, and thus were left out for this intensity map. However, in the polarimetry analysis where POL60 images were included, and the pixels were binned to exchange higher spatial resolution for improvements in the signal-to-noise ratio, this degradation does not significantly affect the results.

3.1. *Morphology*

In the F437M FOC data, the FSC 10214+4724 arc has a length of ∼0.″7 roughly along the east-west direction and is essentially unresolved (<0.″04) in the transverse direction. This is the same basic morphology seen by E96 in the F814W WFPC2 data. The tangential profile exhibits significant structure. Summed over 3 × 3 pixels to improve the signal-to-noise ratio, the arc is seen to have two prominent peaks. The centroids of these two peaks are separated by at least 0.″30. This is significantly larger than the 0.″24 separation observed in the F814W image.

The four objects seen in the F814W image that fall in the FOC field of view are the arc (referred to as component 1 by E96), the two lensing galaxies (components 2 and 3) and the counterimage (component 5). Components 1, 2, and 5 are shown as gray scale and labeled in Figure 1 (*bottom*). The only object visible in the FOC data is the arc, as seen in gray scale in the top panel of Figure 1 and contours in the bottom panel. The absence of components 2 and 3 in the FOC data is expected from their measured spectral energy distributions (E96) and the depth of the FOC image (hereafter, E96's component 2 is referred to as the lensing galaxy). Most significantly, the counterimage seen in the F814W image and in the K band (Graham & Liu 1995; Broadhurst & Lehár 1995) is not present in the F437M FOC data. The ratio of the flux of the arc to the 3 σ level of the background noise at the expected position of the counterimage is 250. This limit is 2.5 times greater than the arc-to-counterimage flux ratio (∼100) in the F814W image (E96).

Our co-added image gives an integrated flux density over the length of the arc of 1.6×10^{-17} ergs cm^{-2} s^{-1} Å^{-1}, equivalent to $B = 21.5$ mag. This is similar to the integrated magnitude obtained by Broadhurst & Lehár.

3.2. *Astrometry*

Astrometry provides critical information needed for mapping the image into the source plane. The task is complicated due to the fact that there is no object other than the arc itself in the FOC field of view. The accuracy of the measurement thus depends upon the knowledge of the distance from the reference object, star A, to the lensing galaxy, and the precision offsetting of *HST*. From the F814W data, Star A was measured to be 13.″19 ± 0.″01 west and 0.″99 ± 0.″02 north of the lensing galaxy. The errors are due to uncertainties in the correction for geometric distortion Mand in the determination of the centroid of star A, whose core is saturated in the F814W PC data. Assuming the telescope pointing between the FOC image of star A and the arc is accurately known, our best determination of the relative positions of the arc at F437M and F814W is shown in Figure 1 (*bottom*). Relative to the I-band arc (in gray scale), the arc as seen by the FOC data (in contours) appears to be shifted radially toward the lensing galaxy, by 12 ± 14 mas. Here we have root sum squared errors of 10 mas the for geometric distortion and centroiding, and 10 mas for telescope pointing (R. Jedrzejewski 1998, private communication).

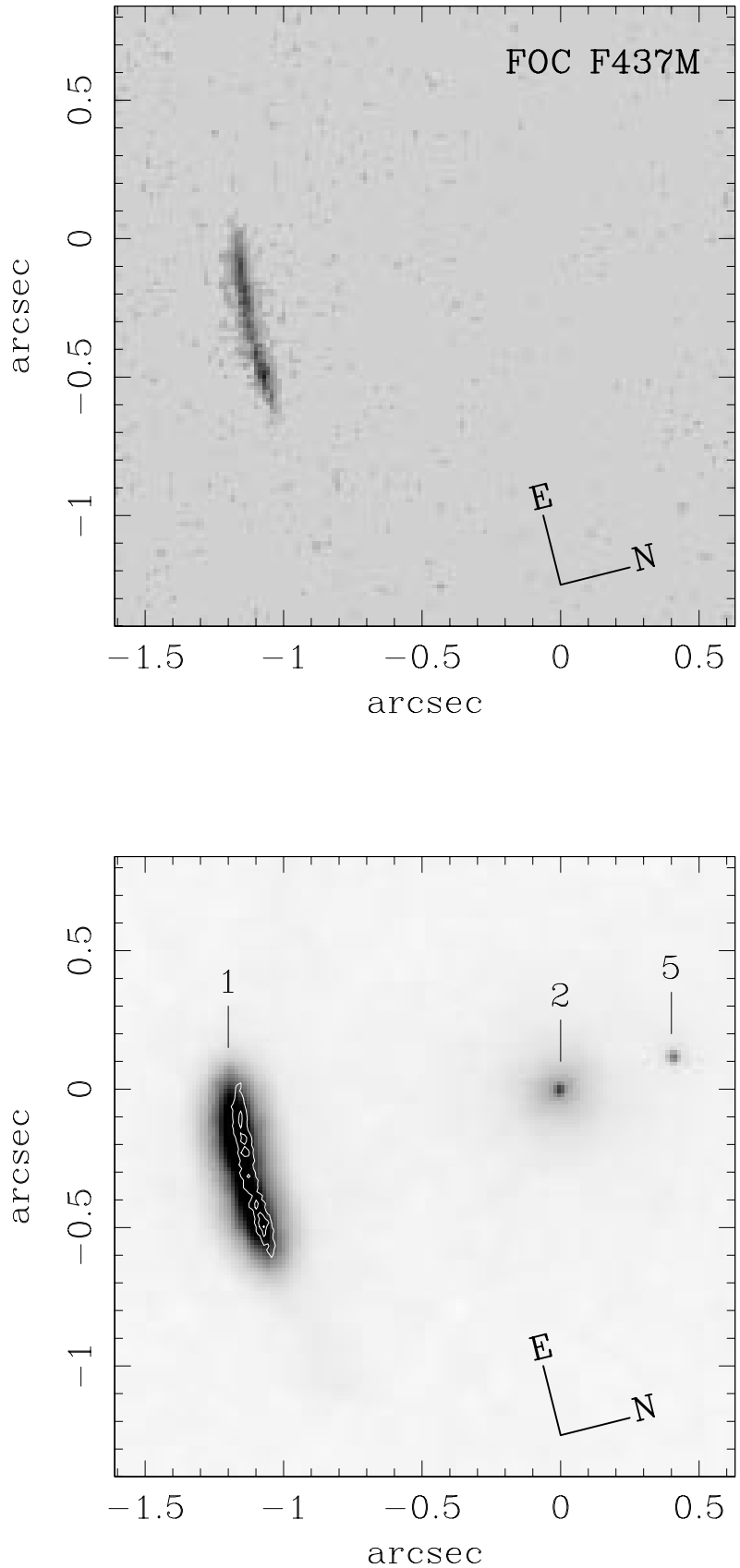

FIG. 1.—*Top*: *HST* Faint Object Camera image of FSC 10214+4724 in filter F437M. (0, 0) is the location of the lensing galaxy as found by E96. North is 76°.0 clockwise from vertical. *Bottom*: Relative astrometry of FSC 10214+4724 at F437M and F814W. The contours are the F437M image and the gray scale is the PC F814W image (E96). The flux of the center pixel of the lensing galaxy and the counterimage in the F814W have been exaggerated in order to be visible. Notice the absence of the F437M contours from the lens galaxy and the counterimage.

3.3. *Polarization*

Our polarization measurement confirms that FSC 10214+4724 is highly polarized. The integrated linear polarization of the entire arc, determined from the total fluxes measured with each of the three polarizers, is 31% ± 3% for the first visit, 24% ± 5% for the second, and 26% ± 5% for the third. The average degree of polarization then is 28% ± 3%, consistent with the ground-based observations (G96). The position angles, measured east of north, for the three separate visits appear to be in satisfactory agreement. They are 59° ± 3°.5 for the first visit, 61° ± 7° for the second, and 67° ± 5° for the third. The overall orientation, after averaging the Stokes parameters from the three visits, is 62° ± 2°.7, compared to the ground-based observations of 69°.9 ± 0°.2 by G96, and 75° ± 3° by Lawrence et al. (1993). Lawrence et al. integrated their polarimetry data over the 400 to 1000 nm range. G96 obtained spectropolarimetry over the same spectral range as Lawrence et al., and their position angle appeared to be constant over that range. The discrepancy in the position angles is not understood, but may be due to inclusion of low surface brightness regions in the ground-based data, which are not detected by *HST*.

Taking advantage of the unresolved nature of the arc in the transverse direction, a high-resolution one-dimensional polarization map was produced by summing over 10 × 3 pixels, in the transverse and tangential directions, respectively. The choice of number of pixels was made so as to improve the signal-to-noise ratio while preserving the structure along the tangential direction. The combination of these pixels gives substantial improvement in signal-to-noise ratio and minimizes the effect of misregistration and differing PSF, thus allowing reliable determination of the polarization for each combined pixel. As shown in Figure 2, the total intensity I, the degree of polarization P, and the position angles vary significantly along the arc. The maximum change in the position angle, $\Delta\theta_{max}$, is 35° ± 5°.

4. DISCUSSION

There are no sources other than FSC 10214+4724 detected in the FOC field of view, even though the image is very deep, with a 3 σ point source detection limit of $B \approx 27.5$ mag in the central 6 × 6 arcsec^2. This is consistent with the expectation from faint field galaxy source counts (Williams et al. 1996).

4.1. *Absence of the Counterimage*

The absence of the counterimage (component 5 in E96) in the *B*-band FOC image is surprising. This may be due either to larger lensing magnification in the F437M bandpass than in F814W seen by E96, or to extinction by dust in the lensing galaxy. We address each of these possibilities in turn.

Although gravitational lensing is achromatic, the magnification is a sensitive function of source size and position near the caustic in the source plane. Different distributions for the UV and optical continuum regions can account for the appearances of FSC 10214+4724 at different wavelengths noted by Matthews et al. (1994). The lens model suggested by E96 and a source geometry as sketched in Figure 3 reproduce qualitatively the inferred lensing magnification of 250, the observed arc morphology and the arc astrometry at F437M. Our source model puts the *B*-band source with a radius of ~20 pc, right on the cusp in the caustic line, approximately 100 pc away from the center of the *I*-band source. The fact that the *B*-band source lies on the caustic is not entirely fortuitous but perhaps due to "magnification bias". In reality the scattering clouds may be widely distributed, but only the regions near the cusp are highly magnified and readily detected. Because of uncertainties in telescope pointing, we take the observed differ-

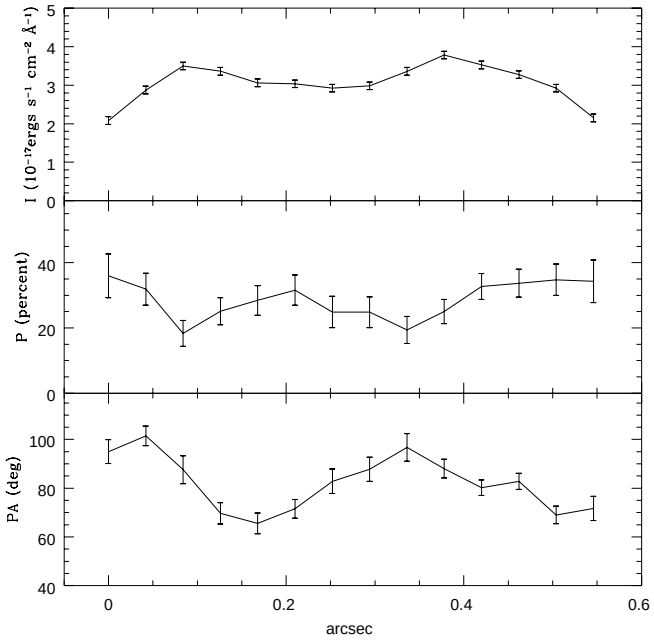

FIG. 2.—One-dimensional profiles of FSC 10214+4724 in filter F437M. Total intensity I (*top*), Degree of polarization P (*middle*), and position angle θ (*bottom*) vs. position in arcseconds along the arc. The smoothing box for the data was 3 pixels parallel to the arc by 10 pixels transverse to the arc. East is to the right.

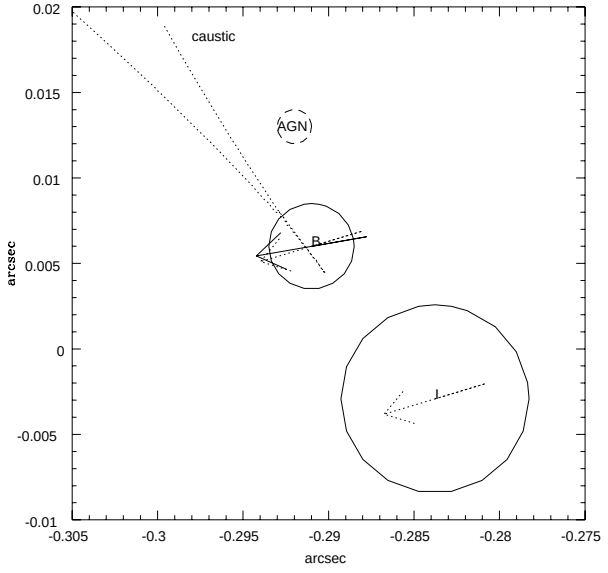

FIG. 3.—Source model of FSC 10214+4724 for lensing magnification of ~250. (*Solid lines*) Position and size of the source in *I* and *B* bands. Solid vector is the position angle measured by this work. Dotted vectors are the position angle measured by G96. (*Broken line*) The caustic. (*Dashed line*) The location of hidden AGN inferred from the variation of the position angles of polarization observed along FSC 10214+4724 arc. (0,0) is the position of the lensing galaxy in the source plane. North is 37°.1 counterclockwise from vertical.

ence in angular position of the arc to be an upper limit rather than a detection. However, the small differences in morphology of the arc, when combined with the lens model, do indeed suggest a small offset between the *B*-band and *I*-band sources, and hence a small offset between the *B*-band and *I*-band arcs of roughly 10 mas, in the direction provided by the telescope astrometry (§ 3.2). For the simple quasar picture in which a scattering cloud is illuminated by a hidden AGN in the source plane, the positional offset of the *B*-band cloud relative to that in the *I* band suggests that the direction from the hidden AGN to these sources could be different, and perhaps could give rise to different position angles (since the polarization vector is perpendicular to the direction to the AGN). However, existing spectropolarimetric data indicate that position angle is independent of wavelength (R. W. Goodrich 1998, private communication).

If in fact there is no radial shift between the *I* and *B* band data sets, reddening in the lensing galaxy may still explain the absence of the counterimage at *B* band, since the counterimage and the arc are viewed through different parts of the elliptical lensing galaxy, and therefore may be affected by different amounts of extinction. Dusty gravitational lenses have been observed (e.g., MG 1131+0534, Larkin et al. 1994; and MG 0414+0534, Lawrence et al. 1995). If it is assumed that the arc is not significantly reddened since its optical path is $\sim$10 kpc away from the center of the lens galaxy, $A_V > 0.67$ mag at $z = 0.9$ is required to produce $E(B-I) > 1$ mag observed for the counterimage, using the extinction law from Cardelli, Clayton, & Mathis 1989 [$R_V = A_V/E(B-V) = 3.1$]. This optical depth is similar to that found in some local elliptical galaxies (Goudfrooij & de Jong 1995). This extinction, if present, would reduce the intrinsic lensing magnification ratio estimated from the F814W data to less than 45, which is closer to the magnification ratio of roughly 30 estimated in the far infrared (E96). The source structure and hence the polarization angle could then be very similar for both F437M and F814W.

4.2. *Pattern of Position Angles*

Given a lensing magnification, it is possible to infer the source diameter, *D*, using a lens model (E96). The observed pattern of position angles then may be directly translated into the source plane and can be used to infer the location of the dust-enshrouded AGN. For the quasar model above, the projected distance, *R*, from the continuum region to the hidden AGN may then be estimated by the simple relation, $D \approx R\Delta\theta_{\max}$, where $\Delta\theta_{\max}$ is the maximum change of the position angle. For a range of lensing magnification from 250 to 45, *D* varies from 40 to 100 pc, so *R* is less than 160 pc (see also, E96). This small scale is generally inaccessible at these wavelengths for objects at redshifts $z > 2$. Notice this range of *R* is similar to the distance from the active nucleus to the continuum region found for the local Seyfert 2 galaxy, NGC 1068 (Capetti et al. 1995).

The relative position of the source and the caustic is crucial in explaining the many features of the arc. For example, if some part of the source is within the cusp, that part will be triply imaged in the arc such that the parity of the first image is opposite to the parity of the second and is the same as that of the third. A monotonic position-angle variation across the source located within the cusp will naturally produce the falling, rising, and falling position angle pattern shown in the central part of Figure 2 (*bottom*).

4.3. *Future Observations*

Either changes in the FSC 10214+4724 source geometry or extinction in the lensing galaxy could be responsible for the fact that the counterimage is present in the *I*-band, WFPC2 data while absent in the *B*-band, FOC data. We expect much of this ambiguity to be resolved by a more accurate determination of the relative astrometry of the FSC 10214+4724 system with planned *HST* WFPC2 observations in F467M and F814W. In the present study, the morphological differences between the unpolarized *I*-band and polarized *B*-band images of FSC 10214+4724 are not large, because the differences in size and location of the regions emitting these components are small relative to the resolution of the high-magnification gravitational lens combined with *HST*. However, the same is not expected to hold for the narrow emission line region (the NLR). From detailed studies of AGNs at low redshifts, it is known that the NLRs and the extended NLRs can exhibit complex morphologies over hundreds of parsecs to kiloparsec scales (e.g., Pogge 1989; Wilson & Tsvetanov 1994). At high redshifts, the emission-line nebula around powerful AGNs can be quite spectacular, reaching sizes of 10–100 kpc (e.g., McCarthy, Spinrad, & van Breugel 1995; Armus et al. 1998). If the NLR of FSC 10214+4724 has similar properties, its appearance through filters isolating specific UV and optical emission lines should be quite different from its broad band, continuum morphology. For example, if the NLR is displaced toward the lensing galaxy, the arc will split up into three images and the counterimage will become relatively more prominent. If displaced away, the arc will become shorter and the counterimage will again become relatively more prominent. The displacement, shape and size of the NLR may be determined from the observed morphology and the lens model. This makes FSC 10214+4724 a unique system for direct imaging of quasar emission regions at high redshift. Observations are planned in *HST* cycle 7 to image this system in narrowband filters centered on the narrow emission lines, [C IV] λ1549, [Ne V] λ3426, and [O III] λ5007.

5. SUMMARY AND CONCLUSIONS

We have reported imaging polarimetry of the gravitationally lensed object FSC 10214+4724, carried out with 0.″04 resolution at F437M (roughly *B* band) using the Faint Object Camera on *HST*. The principal results of this work are the following:

1. The F437M source appears as an unresolved arc, 0.″7 × <0.″04, coincident to within the errors with the arc seen at F814W by E96.

2. The absence of a counterimage suggests that the apparent magnification at F437M is greater than 250, considerably higher than measured at F814W and inferred for the far infrared (E96). It is possible that this effect is due to differential extinction in the lensing galaxy ($A_v > 0.67$). However, if further work shows that the magnification is in fact higher at F437M than at F814W, then the emitting region at the shorter wavelength must be smaller and closer to the caustic of the lensing potential. The size and position difference might be a consequence of patchy UV extinction in the high-luminosity core of FSC 10214+4724 (Lacy et al. 1998).

3. The net polarization of the arc at F437M is consistent with what has been determined from ground-based mea-

surements, but we determine that the position angle of polarization rotates systematically with position along the arc. The total variation of the angle is about 35°. Under the assumption that the polarization is due to scattering of continuum radiation from an embedded source, the projected distance of the scattering region from this source is less than 160 pc; it could be as small as 60 pc if the magnification is in fact as high as 250.

We thank Roger Blandford and Roger Hildebrand for helpful discussions and Robin Evans for his help with corrections for geometrical distortion of the PC data. H. T. N. wishes to thank the Institute for Advanced Study for its hospitality during his visit for a part of this work. Support for D. W. H. was provided by Hubble Fellowship grant HF-01093.01-97A from STScI, which is operated by AURA under NASA contract NAS 5-26555. Support for this work was provided by NASA through grant number GO-6834.01-95A from STScI, which is operated by AURA under NASA contract NAS 5-26555. Portions of the research described in this paper were carried out by the Jet Propulsion Laboratory, California Institute of Technology, under a contract with NASA.

REFERENCES

Armus, L., Soifer, B. T., Murphy, T. W., Jr., Neugebauer, G., Evans, A. S., & Mathews, K. 1998, ApJ, 495, 276
Broadhurst, T., & Lehár, J. 1995, ApJ, 450, L41
Capetti, A., Axon, D. J., Macchetto, F., Sparks, W. B., & Boksenberg, A. 1995, ApJ, 446, 155
Cardelli, J. A., Clayton, G. C., & Mathis, J. S. 1989, ApJ, 345, 245
Downes, D., Solomon, P. M., & Radford, S. J. E. 1995, ApJ, 453, L65
Eisenhardt, P. R., Armus, L., Hogg D. W., Soifer, B. T., Neugebauer, G., & Werner, M. W. 1996, ApJ, 461, 72 (E96)
Goodrich, R. W., Miller, J. S., Martel, A., Cohen, M. H., Tran, H. D., Ogle, P. M., & Vermeulen, R. C. 1996, ApJ, 456, L9 (G96)
Goudfrooij P., & de Jong T. 1995, A&A, 298, 784
Graham, J. R., & Liu, M. C. 1995, ApJ, 449, L29
Kroker, H., Genzel, R.,. Krabbe, A., Tacconi-Garmant, L. E., Tecza, M., Thatie, N., & Beckwith, S. V. W. 1996, ApJ, 463, L55
Lacy, M., Rawlings, S., & Serjeant, S. 1998, MNRAS, 299, 1220
Larkin, J. E., et al. 1994, ApJ, 420, L9
Lawrence, A., et al. 1993, MNRAS, 260, 28
Lawrence, C. R., Elston, R., Januzzi, B. T., & Turner, E. L. 1995, AJ, 110, 2570
Matthews, K., et al. 1994, ApJ, 420, L13
McCarthy, P. J., Spinrad, H., & van Breugel, W. 1995, ApJS, 99 27
Pogge, R. W. 1989, ApJ, 345, 730
Rowan-Robinson, M., et al. 1991, Nature, 351, 719
Rowan-Robinson, M., et al. 1993, MNRAS, 261, 513
Scoville, N. Z., Yun, M. S., Brown, R. L., & Vanden Bout, P. A. 1995, ApJ, 449, L109
Thompson, R. C., & Robinson, D. R. T. 1995, ST-ECF Newslett., 23, 33
Williams, R. E., et al. 1996, AJ, 112, 1335
Wilson, A. S., & Tsvetanov, Z. I. 1994, AJ, 107, 1227